

Surface Ablation of Dielectrics with sub-10 fs to 300 fs Laser Pulses: Crater Depth and Diameter, and Efficiency as a Function of Laser Intensity

O. Utéza*, N. Sanner*, B. Chimier*, M. Sentis*, P. Lassonde**, F. Légaré**, J.C. Kieffer**

* Laboratoire LP3, UMR 6182 CNRS – Université de la Méditerranée,
C. 917, 163, Av. de Luminy, 13288 Marseille cedex 9, France
E-mail: uteza@lp3.univ-mrs.fr

** INRS, Energie, Matériaux et Télécommunications, 1650 bld Lionel Boulet, Varennes (Québec),
Canada, J3X 1S2

Surface ablation of a dielectric material (fused silica) is studied as a function of pulse duration (< 10 fs – 300 fs) and applied fluence ($F_{th} < F < 10 F_{th}$) using single femtosecond pulse. We show that the axial selectivity (crater depth) depends on the applied intensity while the transverse selectivity (crater diameter) only depends on the applied fluence. The ablation efficiency, expressed in $\mu\text{m}^3/\mu\text{J}$, is shown to be inversely proportional to the pulse duration and saturates with respect to the applied fluence earlier at short pulse durations (≤ 30 fs). The deduced optimal fluence F_{opt} , corresponding to the highest ablation efficiency for each pulse width, defines two regimes of laser application, characterized either by high selectivity ($F < F_{opt}$) or high control ($F > F_{opt}$) of ablation characteristics.

Keywords: Ultrashort pulses, dielectrics, surface ablation, crater depth and diameter, efficiency

1. Introduction

Femtosecond laser pulses provide unique advantages for high precision processing of both metals and dielectric materials [1-3]. In particular, femtosecond irradiation provides minimization of collateral damages, reduction of heat-affected zone, deterministic damage behavior, and ability to machine sub-diffraction limited target regions. These advantages facilitate the development of numerous applications such as ultra-precise laser treatment, laser surgery, and industrial micromachining (micro-fabrication and micro-transformation) [1-6].

In this paper, we study the physical characteristics of surface ablation craters in fused silica created by direct laser interaction with sub-10 fs to 300 fs single laser pulse (800 nm). These investigations aim to provide knowledge and control over important parameters as a function of applied intensity in femtosecond regime, such as ablation threshold fluence, crater depth and diameter, and ablation efficiency. This information is of crucial importance for finalizing any laser-based micromachining processes and for laser-matter technology in general.

2. Experiments

Experiments are performed using a KMLabs laser source delivering linearly polarized 25 fs - 5 kHz pulses at 800 nm (see Fig. 1). Self phase modulation (SPM) in a hollow-core fiber (HF) filled with Argon generates a wide spectrum recompressed by chirped mirrors to reach bandwidth-limited 7 fs pulses. 30 fs pulses are obtained by replacing Argon with Helium such that SPM is completely suppressed. 100 fs pulses are obtained by limiting the spectrum width in the compressor of the commercial 25 fs source, whereas 300 fs pulses are produced by introducing a controlled chirp with an acousto-optic filter inside the laser chain. The HF also acts as a spatial filter, selecting only the fundamental mode. In order to get clean temporal pulse

profile free of wings or residual satellite peaks, the spectral phase of the pulse emitted by the laser source is initially controlled by a Spider. The residual inverse spectral phase is then generated by means of a Dazzler system to get nearly Fourier-Transform limited pulses before performing any spectrum modulation. Afterwards, the final pulse profile, before being focused on the sample, is controlled by second-order autocorrelation measuring its pulse duration. In addition, at 30 and 100 fs, the coherent contrast was measured using a third order autocorrelation system yielding a contrast at 2 ps before the main pulse in excess of 10^6 . The combination of a half-wave plate and a pair of reflective Germanium plates at the Brewster angle enables variable attenuation to control finely the pulse energy incident on the target sample. The beam is focused by an off-axis parabolic mirror of 50 mm focal length, leading to a focal spot of radius $w_0=4.65 \mu\text{m}$ at $1/e^2$ (measured by imaging on a CCD camera) with a nearly-Gaussian intensity distribution.

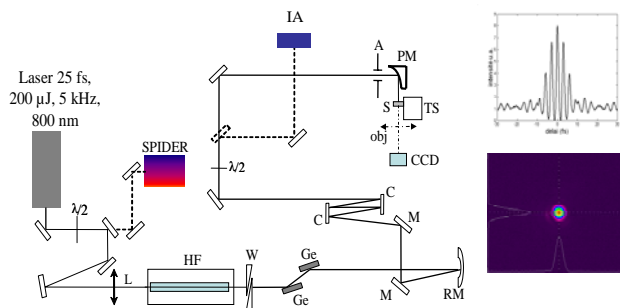


Fig. 1 Experimental set-up: Laser damage/ablation test bench with spatial (camera, CCD) and temporal (autocorrelator, IA) diagnostics. HF: hollow-core fiber; W: wedge plate; Ge: Germanium Brewster polarizer; M: mirror; RM: recollimation mirror; C: chirped mirror; A: Iris aperture; PM: parabolic mirror; TS: translation stage; S: sample.

The laser fluence F is expressed by $F = 2E/\pi w_0^2$, considering the local peak fluence. The targets are high-purity superpolished fused silica (a-SiO₂ Suprasil from Heraeus, bandgap: $E_g=8.9$ eV) with impurity <0.065 ppm and residual roughness $R_a=0.2$ nm. Precise positioning of the target surface at the focal plane is obtained by combined energy-scan and z-scan procedures. All the experiments are performed under ambient air *in single shot regime*, ensured by the fast translation of the sample (25 cm/s) in front of the 5 kHz laser beam. The interval between adjacent damages is 50 μm , which is ~ 5 times larger than the largest damages, so that contamination by possible redeposition of debris in a neighbour impact is prevented.

3. Ablation Characteristics: Results and discussion

Figure 2 presents the evolution of the ablated volume as a function of the peak laser fluence F and for a large set of pulse durations. The vertical error bars correspond to the deviation observed on AFM measurements of five independent ablation tests. Their magnitude tends to increase with the applied fluence for all pulse durations. A linear rise of the ablated volume with the pulse fluence is observed at low fluences before weak saturation begins to occur. Extrapolating the linear regression to zero allows inferring the ablation threshold F_{th} for each studied case [7]. The evolution of the ablation threshold as a function of pulse duration is discussed in other papers [8,9] and we focus here on the analysis of ablation characteristics.

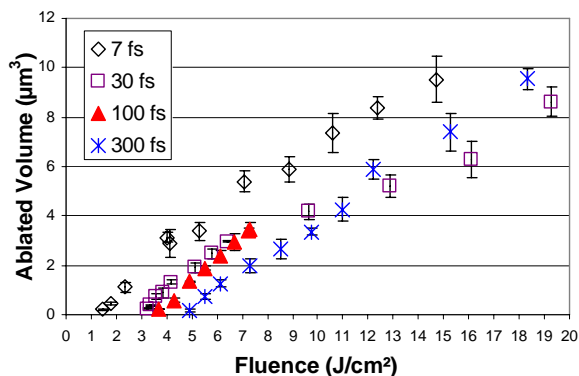


Fig. 2 Volume ablated versus applied fluence and for different pulse durations (7, 30, 100, 300 fs).

Figure 3a-c then regroups the evolution of the ablated volume, crater depth (maximum depth of the irradiated zone) and normalized diameter ($D/\pi w_0$) as a function of normalized fluence F/F_{th} and pulse duration. The crater diameter D is normalized with respect to the full beam size (99% of energy) equal to πw_0 . Clearly, we again distinguish different regimes of interaction, with an initial linear increase of the ablation characteristics at low and moderate fluences ($F \leq 2 F_{th}$) further followed by a partial or complete saturation at higher fluences ($F > 2 F_{th}$). Note that the saturation effect is more pronounced for very short pulse durations (≤ 30 fs) and especially when considering the crater depth evolution versus fluence. This evolution is attributed to the development of the plasma formed in a thin surface layer of the sample, becoming gradually overcritical at the beam centre and reflecting the late part of the beam [2,10]. In other words, the plasma formed acts as an ultrafast shutter with a

switching (closing) time being shorter and more efficient when the pulse duration decreases. Indeed, considering Fig. 3b, it can be seen that the crater depth saturation is complete for $F > 2 F_{th}$ while it is only partial for long pulses at high fluences. When using very short pulses, the rapid creation of high density free electron plasma is due to the efficiency of photo-ionization [see for instance 11]. For long pulses (≥ 100 fs), the saturation is not complete (partial closing of the ultrafast optical shutter) due to the smaller free electron growth rate (smaller applied intensity) and the long time required to obtain a sufficiently high free electron density through avalanche ionization. Nevertheless a significant optical shutter effect is also expected to occur at very high applied fluences when using “long” femtosecond pulses.

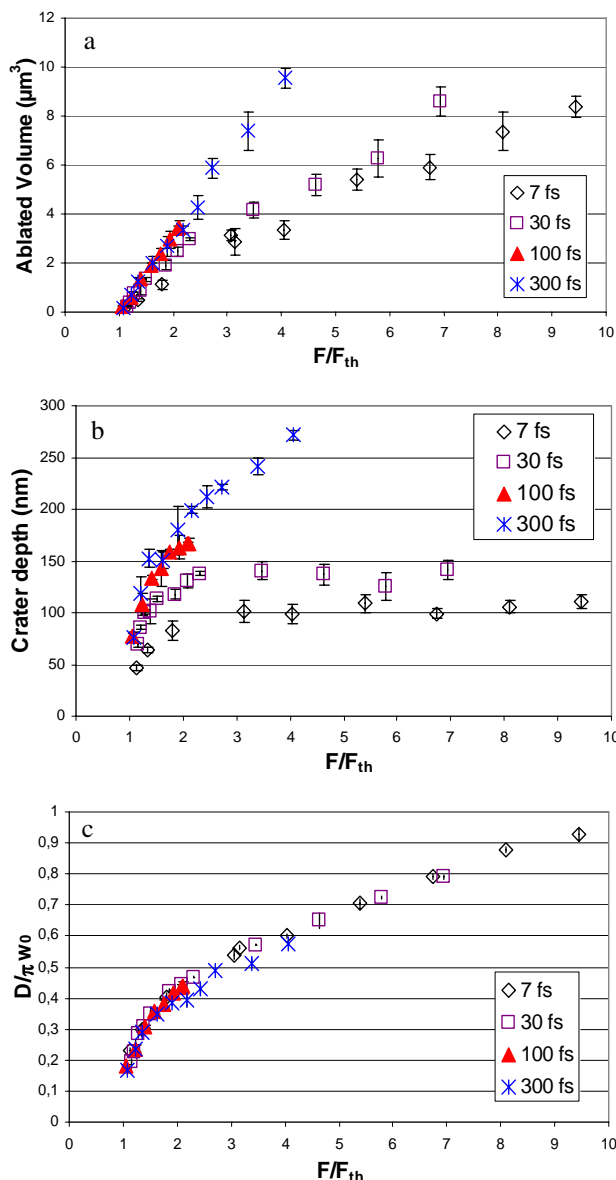


Fig. 3 Volume ablated (a), crater depth (b) and normalized diameter $D/\pi w_0$ (c) versus normalized fluence and pulse duration.

Note that another phenomenon could also contribute to the observed behaviour. This phenomenon deals with laser-induced ionization of the ambient air taking place just be-

fore the sample and thus leading to beam defocusing. However, this effect is expected to occur at high intensity ($\geq 5 \times 10^{14}$ W/cm²) [12], mainly here at very short pulse duration (≤ 30 fs) and high fluences. Simulation are today in progress to estimate the importance of this effect on the beam propagation and on the ablation characteristics observed at very high intensities.

The electronic density being smaller at the edges of the irradiated zone due to the lower applied fluence (pulse with spatial Gaussian distribution), the energy deposition is not stopped at the beam borders. Thus, the crater size (see Fig. 3c) and as a consequence the ablated volume (see Fig. 3a) continue to increase at high fluences ($F > 2 F_{th}$). On a practical point of view, we therefore conclude that the axial resolution (crater depth) depends on the normalized intensity I/I_{th} while the transverse ablation resolution (crater diameter), only depends on the normalized applied fluence F/F_{th} . This deduction is crucial for micromachining applications, for which knowledge of the amount of material removal per unit energy and aspect ratio (crater diameter and depth) are essential information. The ablation efficiency, defined as the ratio of the ablated volume to the incident energy is then plotted on Figure 4. The ablation efficiency is shown to be inversely proportional to the pulse duration and to saturate with respect to the applied fluence earlier at short pulse durations (≤ 30 fs).

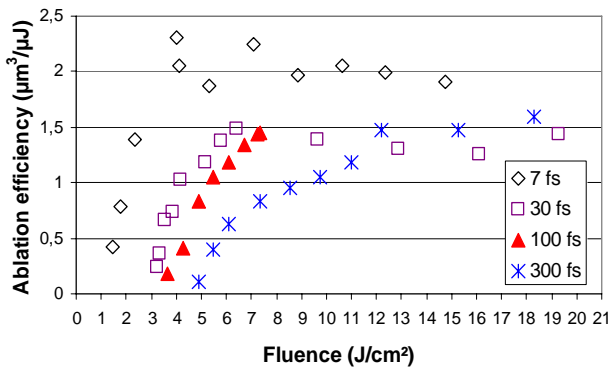


Fig. 4 Ablation efficiency versus applied fluence and for different pulse durations.

An optimal fluence F_{opt} (correspondingly optimal intensity I_{opt}) can be determined for all pulse durations, corresponding to the maximum value of ablation efficiency (see Fig. 4). According to our results, optimum fluences F_{opt} are determined for 7, 30 fs and 300 fs, while lack of data at 100 fs precludes a precise estimation of this parameter (see Table 1). The optimum intensity I_{opt} is shown to be higher as the pulse duration is shorter. However, the increase of I_{opt} at short pulse duration does not occur in proportion of the reduction of the pulse duration. This point to be remarked will be discussed in details in a forthcoming paper.

For $F_{th} < F < F_{opt}$, the slope of ablation efficiency is positive and the ablation highly selective. For instance, a high selectivity (~ 10 nm) in removal of matter thickness can be reached (see Fig. 3b). Varying the pulse duration allows accessing different depth ranges from $\sim 40 - 150$ nm for very short pulses (≤ 30 fs) to $\sim 60 - 300$ nm for longer pulses, giving versatility to femtosecond laser sources for which the pulse duration can be easily tuned. In the same

time, calibrated removal of small amounts of material ($\sim 0.2 \mu\text{m}^3/\mu\text{J}$) can be accessed close to the ablation threshold F_{th} .

Table 1 F_{opt} and I_{opt} as a function of pulse duration. F_{th} is also given for information.

Pulse duration (fs)	F_{th} (J/cm ²)	F_{opt} (J/cm ²)	I_{opt} (W/cm ²)
7	1.3	4	5.7×10^{14}
30	2.8	6.4	2.1×10^{14}
100	3.5	> 7.3	$> 7.3 \times 10^{13}$
300	4.5	12.2	4.05×10^{13}

However, “the price to pay” for calibration and selectivity is to dispose of a stable laser. In our conditions, a laser having $\sim 3\%$ rms energy fluctuations was used. However, we think that higher removal resolution and selectivity could be obtained with a laser more stable due to the highly deterministic behaviour observed with femtosecond pulses, especially at very short pulse durations [8,13]. Moreover, the “selective processing fluence window” is shown to be more extended at long pulse durations ($\gg 30$ fs) (see Fig. 5) due to the later onset of the plasma shutter effect.

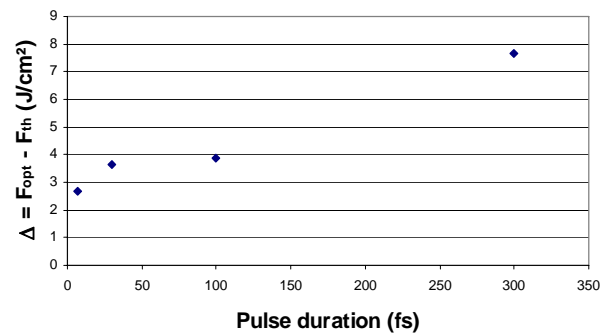


Fig. 5 Evolution of the magnitude of selective work fluence window $\Delta = F_{opt} - F_{th}$ as a function of pulse duration.

However, the precision of the ablation is slightly lower as the shot-to-shot fluctuations observed on the ablation characteristics (ablated volume, crater depth and size) tend to increase with the pulse duration. In addition, the surface quality of the processed zone appears to be also worse when using long femtosecond pulses (≥ 100 fs) as the crater morphology shows evidence of thermo mechanical stress (elevated rim) (Fig.6) whatever the incident fluence. In comparison, the crater morphology is free of any significant thermo mechanical effects when working with ultrashort laser pulses and close to the threshold fluence (Fig. 7). However, at higher fluences, a thin and slightly elevated rim also appears but the ablated profiles remain remarkably regular and smooth in this temporal regime.

For $F > F_{opt}$, we observe a saturation of the ablation efficiency followed by a progressive decrease. In this regime, the magnitude of matter removal is high ($> 1.5 \mu\text{m}^3/\mu\text{J}$) for all pulse durations and large calibrated matter removal is easily achieved due to the beginning of saturation of crater depth with the applied fluence. This working fluence range is then favourable when highly controlled process is

searched. However the quality of process (heat-affected zone, morphology degradation) is expected to diminish with respect to laser process close to the ablation threshold due to more intense thermo-mechanical effects occurring at large applied fluences (higher energy deposition). The increase in the magnitude of the error bars observed on figures 2 and 3 at high fluences confirms this tendency.

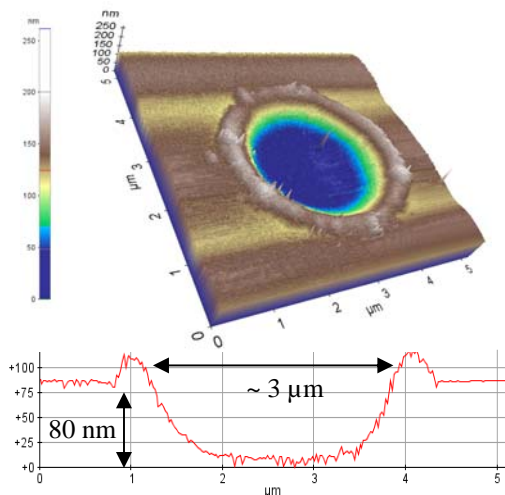


Fig. 6 AFM 3D (above) and 1D (bottom) profiles obtained at 100 fs and close to the ablation threshold ($\sim 1.1 F_{th}$).

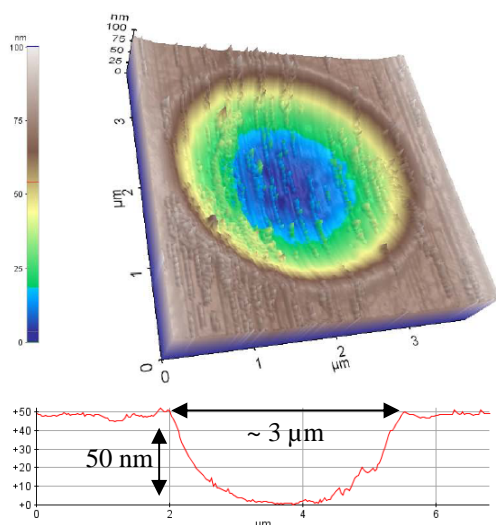


Fig. 7 3D (above) and 1D (bottom) AFM profiles obtained at ultrashort pulse duration (7 fs) and close to the ablation threshold ($1.1 F_{th}$).

4. Conclusions

These investigations provided experimental knowledge over important laser ablation parameters of micrometer scale in dielectrics (SiO_2) like removed volume, thickness, processed diameter and efficiency as a function of applied laser intensity using single shot femtosecond pulse (7 – 300 fs). In particular, we showed that it is possible to access different ranges of axial selectivity (crater depth) with a precision of ~ 10 nm by selecting different pulse durations while the transverse selectivity (crater diameter) only depends on the applied fluence. The ablation efficiency is

shown to be inversely proportional to the pulse duration and saturates with respect to the applied fluence earlier at short pulse durations (≤ 30 fs). The deduced optimal fluence F_{opt} corresponding to the highest ablation efficiency for each pulse width defines two regimes of laser application. Below F_{opt} , the material removal can be highly selective as a function of the applied fluence. Above F_{opt} , the material removal is little selective but particularly easy to control. These results can serve as guidelines for the choice of laser parameters in the frame of industrial development of femtosecond micromachining processes.

Acknowledgments

This research was financially supported by the French National Agency of Research (ANR) under contracts “Festic-ANR-06-BLAN-0298-02” and “Nanomorphing-ANR-07-BLAN-0301-03” and by the Region Provence-Alpes-Côte d’Azur and Department of Bouches-du-Rhône.

References

- [1] R. Gattass and E. Mazur: *Nat. Phot.*, 2, (2008), 219.
- [2] M. Perry, B.C. Stuart, M.D. Feit, A.M. Rubenchik, V. Yanovsky: *J. of Appl. Phys.*, 85 (9), (1999) 6803
- [3] B.N. Chichkov, C. Momma, S. Nolte, F. Von Alvensleben, A. Tünnermann: *Appl. Phys. A*, 63, (1996) 109
- [4] S.H. Chung and E. Mazur: *J. of Biophoton.*, 2 (10), (2009), 557.
- [5] S. Juodkazis, V. Mizeikis, H. Mizawa: *J. of Appl. Phys.*, 106, (2009), 051101.
- [6] “Laser Ablation and its Applications” edited by C.R. Phipps (Springer Series in Optical Sciences, Springer, New-York, 2007), Part 2: Ultrafast Interactions.
- [7] N. Sanner, O. Utéza, B. Bussiere, G. Coustillier, A. Leray, T. Itina, M. Sentis: *Appl. Phys. A*, 94, (2009), 889.
- [8] N. Sanner, O. Utéza, B. Chimier, M. Sentis, P. Lassonde, F. Légaré, J.C. Kieffer: *Appl. Phys. Lett.*, 96, (2010), 071111.
- [9] T. Itina, O. Utéza, N. Sanner, M. Sentis: *Journal of Optoelectronics and Advanced Materials*, 12 (3), (2010), 470.
- [10] M.D. Feit, A.M. Komashko, A.M. Rubenchik: *Appl. Phys. A*, 79, (2004), 1657.
- [11] A.C. Tien, S. Backus, H. Kapteyn, M. Murnane, and G. Mourou: *Phys. Rev. Lett.*, 82 (19), (1999), 3883.
- [12] A.A. Ionin, S.I. Kudryashov, L.V. Seleznev, D.V. Sinitsyn: *JETP Letters*, 90 (3), (2009), 181.
- [13] A. P. Joglekar, H. Liu, G. J. Spooner, E. Meyhofer, G. Mourou, A. J. Hunt: *Appl. Phys. B*, 77, (2003), 25.

(Received: June 7, 2010, Accepted: November 16, 2010)